On the signature of the quasi-3-day wave in the thermosphere during the January 2010 URSI World Day Campaign

Scott L. England,[1] Guiping Liu,[1] Qihou Zhou,[2] Thomas J. Immel,[1] Karanam K. Kumar,[3] and Geetha Ramkumar[3]

Received 24 January 2012; revised 2 April 2012; accepted 24 April 2012; published 5 June 2012.

[1] Ultra-fast Kelvin waves with periods of 3–5 days are important in the coupling of the lower atmosphere to the thermosphere and ionosphere. Here we focus on the observations and effects of a 3-day wave during January 2010. As this time period coincides with a stratospheric warming event, a coordinated set of observations with incoherent scatter radars are available. While there is no evidence that the occurrence of this 3-day wave is connected with this event, these observations offer an unprecedented glimpse of the thermospheric conditions during this period, including the first-ever detection of a 3-day wave with an incoherent scatter radar. Using a combination of ground- and space-based observations, we identify an eastward moving zonal wave number-one 3-day equatorial wave that is comprised of a Kelvin wave at the lowest latitudes and a Rossby-gravity wave at higher latitudes. In the equatorial region, the vertical wavelength is ∼40 km and the wave peaks in amplitude around 95–100 km altitude. The wave observed here is only seen to propagate to around 105 km altitude. Evidence of an interaction between this wave and the diurnal tide is seen between 82–88 km. The resultant 3-day periodicity in the diurnal tide is seen to propagate up to altitudes of ∼150 km. This could have a significant impact on the ionosphere via modulation of the E-region dynamo, thus carrying the 3-day periodicity to higher altitudes.

Citation: England, S. L., G. Liu, Q. Zhou, T. J. Immel, K. K. Kumar, and G. Ramkumar (2012), On the signature of the quasi-3-day wave in the thermosphere during the January 2010 URSI World Day Campaign, *J. Geophys. Res.*, *117*, A06304, doi:10.1029/2012JA017558.

1. Introduction

[2] Planetary-scale atmospheric waves are believed to play a central role in the vertical coupling of the atmosphere and ionosphere. Recently, such waves and their impacts on the upper atmosphere and ionosphere have been the focus of much research, with particular interest in (1) the persistent longitudinal variations in the low-latitude ionosphere associated with the non-migrating tides (see *England* [2012] for a recent review), (2) periodic temporal variations in the ionosphere [*Pancheva et al.*, 2002; *Fagundes et al.*, 2005; *Pancheva et al.*, 2006; *Takahashi et al.*, 2006, 2007; *Fagundes et al.*, 2009a, 2009b; *G. Liu et al.*, 2010a; *Chang et al.*, 2010; *G. Liu et al.*, 2010b; *Bertoni et al.*, 2011] and (3) the response to significant atmospheric events such as stratospheric sudden warmings (SSW hereafter; see *Chau et al.* [2012] for a recent review).

[3] Kelvin waves are one class of these waves that are believed to be generated by latent heat release in the troposphere [*Holton*, 1973; *Salby and Garcia*, 1987] and are believed to be important in the connection of this lower atmosphere wave source to the upper atmosphere and ionosphere. These waves are trapped in the equatorial region and propagate eastward with respect to the background flow. The idealized description of Kelvin waves [e.g., *Andrews et al.*, 1987] shows that they are characterized by wind perturbations in the zonal direction only, but away from the equator the beta-plane approximation on which such descriptions are based breaks down and some non-zero meridional wind component is often observed [e.g., *Riggin et al.*, 1997]. There are three distinct classes of Kelvin waves that have been observed. The longest period, 'slow' Kelvin waves have periods in the range of 15–20 days [*Wallace and Kousky*, 1968]. These have short vertical wavelengths (∼10 km) and are unable to propagate above the stratosphere. 'Fast' Kelvin waves have periods in the range of 6–10 days [*Hirota*, 1979] and larger vertical wavelengths (∼20 km). 'Ultra-fast' Kelvin waves (UFKW hereafter) have the shortest periods (∼3–5 days [*Salby et al.*, 1984]).

[4] From wind observations made with UARS-HRDI, *Lieberman and Riggin* [1997] showed the UFKW can have

[1]Space Sciences Laboratory, University of California Berkeley, Berkeley, California, USA.
[2]Electrical and Computer Engineering Department, Miami University, Oxford, Ohio, USA.
[3]Space Physics Laboratory, Vikram Sarabhai Space Center, Trivandrum, India.

Corresponding author: S. L. England, Space Sciences Laboratory, University of California, Berkeley, CA 94720, USA. (england@ssl.berkeley.edu)

0148-0227/12/2012JA017558

zonal wave numbers 1–3, with wave number-1 being the most commonly observed. They occur sporadically, with the greatest occurrence rates around January-February and June–August [*Vincent*, 1993; *Yoshida et al.*, 1999; *Davis et al.*, 2011]. The most common wave number-1 UFKW has a zonal phase velocity ∼150 ms^{-1}. This, combined with a vertical wavelength of ∼40 km allows them to propagate into the thermosphere [*Forbes*, 2000]. As the background density decreases with altitude, their amplitudes tend to increase and peak around ∼105 km [*Lieberman and Riggin*, 1997], but these waves have been observed to propagate to ∼120 km by TIMED-SABER [*Forbes et al.*, 2009]. In the lower thermosphere, these waves can reach peak zonal wind amplitudes of 10–40 ms^{-1}, making them perhaps the most important of the Kelvin waves for the dynamics of the upper atmosphere and ionosphere.

[5] Even during geomagnetic- and solar-quiet conditions, the ionosphere displays a remarkable amount of day-to-day variability. *Forbes* [2000] showed that for even the quietest conditions ($K_p \leq 1$), the density of the ionospheric peak (N_{max}) has a standard deviation of 15–30% on time-scales of 2–30 days at all latitudes. One likely source of some of this variability is the influence of planetary waves and UFKWs, whose periods fall within this range. From coincident ground based radar observations of the mesosphere and F-region ionosphere, *Takahashi et al.* [2006, 2007] showed that the height and density of the F-layer peak displayed a 3-day periodicity that was coincident with the presence of a 3-day UFKW in the mesosphere. The authors suggested that this could be the result of either the perturbation of the E-region dynamo by the UFKW or direct propagation of that wave to F-region altitudes. While the ability of the UFKW to propagate to F-region altitudes is supported by numerical studies such as *Chang et al.* [2010], other simulations have suggested that these waves should dissipate below these altitudes [e.g., *Pogoreltsev et al.*, 2007]. Using the TIME-GCM model, *Chang et al.* [2010] investigated the potential coupling mechanisms between the UFKW and its signature in the ionosphere. The authors showed that while the UFKW propagate up to F-region altitudes in this model, its modification of the E-region dynamo was the primary source of the accompanying 3-day modulation of the F-region ionosphere. Further, while the UFKW was seen to interact with tides in the model resulting in the production of 'child-waves', the authors concluded that these did not make a significant contribution to the 3-day modulation of the ionosphere.

[6] Here we present observations of a 3-day equatorial wave that coincides approximately with the late January 2010 onset of a SSW. The occurrence of such waves is relatively common during January and there is no indication that this occurrence is linked with the SSW. Indeed, the 3-day wave is first seen several days before the onset of the SSW. However, as there has been a recent concerted effort to define the impact of these events on the mesosphere, lower thermosphere and ionosphere [see *Chau et al.* [2012] for a recent review), including the coordinated observations made with multiple incoherent scatter radars (ISR) through URSI World Day campaigns [*Goncharenko and Zhang*, 2008], the data available during this period offer a rare glimpse of equatorial-wave activity in the lower thermosphere. Section 2 describes the data from the SKiYMET radar at Thumba, Arecibo ISR, TIMED-TIDI and TIMED-SABER that will be used in this investigation. Section 3 describes the ground- and space-based observations of the characteristics of the 3-day wave. Section 4 describes the interaction of the 3-day wave with the diurnal tide in the mesosphere and the resultant periodic variation of the diurnal oscillation in the lower thermosphere.

2. Data

2.1. Neutral Wind Measurements Made by the SKiYMET Radar at Thumba

[7] Ground-based observations of the neutral winds in the equatorial MLT region offer an ideal way to identify planetary wave periodicities in the neutral atmosphere. Here we use observations from the All-Sky Interferometeric Meteor (SKiYMET) radar at Thumba, India, which is located on the magnetic equator. This radar is able to measure the neutral winds from ∼80–100 km altitude in 3 km altitude bins [*Kumar et al.*, 2007] and has been used for numerous studies of planetary wave activity (recent examples are *G. Liu et al.* [2010a, 2010b]). The data used here (as in these previous studies) are hourly mean values of the horizontal wind.

2.2. Meridional Wind Measurements Made by the Arecibo ISR

[8] The Arecibo ISR is capable of measuring the power spectra resulting from the fluctuations of the ionosphere from ∼60–2000 km [e.g., *Isham et al.*, 2000]. The Arecibo ISR has a number of operating modes, but most relevant to our discussion here are the data taken using the radar's Coded Long Pulse (CLP) and Power modes [*Isham et al.*, 2000]. Using these data, it is possible to determine a number of parameters, such as the ion temperature, and owing to the availability of the coplanar dual beam at Arecibo since the late 1990s [*Aponte et al.*, 2005], it is also possible to derive the horizontal wind at thermospheric altitudes [*Zhou et al.*, 1997b]. As demonstrated by *Zhou et al.* [1997b], both zonal and meridional winds at E-region altitudes can be found from the observations of the vector ion drifts made by the Arecibo ISR, each relying upon different assumptions. The derivation of the zonal winds requires knowledge of the ion-neutral collision frequency, ion mass and zonal electric field at E-region altitudes. The ISR is able to provide a measure of the electric field, but is unable to the estimate of the ion-neutral collision frequency and ion mass. Therefore, the MSIS empirical model [*Hedin*, 1992] is typically used. As the ISR is unable to provide estimates of these parameters on the time-scales required [*Zhou et al.*, 1997b], the uncertainties in the zonal winds above ∼112 km are large and not quantified. For this reason, the present study will only consider the meridional winds derived from the Arecibo ISR. The meridional winds are also derived from the measured ion drifts, but require only knowledge of the Earth's magnetic field and the assumption that the vertical winds are small [*Zhou et al.*, 1997b]. Under normal conditions, the hourly-averaged vertical neutral winds in the equatorial lower thermosphere can be considered negligible against the meridional winds. However, as the ratio of these two wind components is not known, a formal error analysis of the meridional winds from Arecibo is not possible. Therefore, rather than considering the errors in the derived winds, we use the coherence in the periodograms between

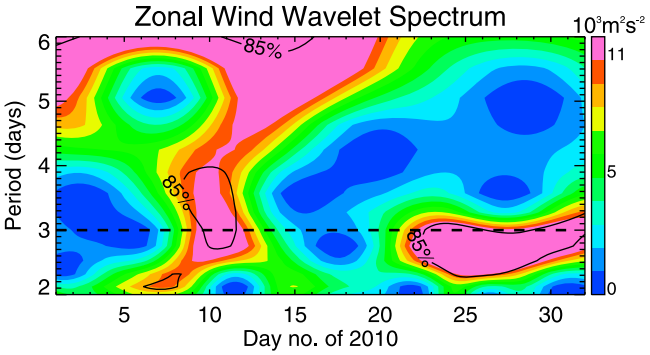

Figure 1. Wavelet power spectrum of hourly mean zonal wind measurements by the SKiYMET radar at Thumba for 98 km altitude during January 1–31, 2010. The black contour lines mark the 85% significance level of the wavelet spectrum. Note, data from December 1, 2009 to February 28, 2010 were used in the analysis to avoid wavelet edge effects.

adjacent altitude levels (each of which is calculated independently) as a gauge of the confidence in the periodic signatures found using Arecibo.

2.3. Horizontal Wind Measurements Made by TIMED-TIDI

[9] The TIMED Doppler Interferometer (TIDI) measures neutral winds in the region MLT [*Killeen et al.*, 2006]. TIDI regularly obtains wind measurements in the ~80–115 km altitude range [e.g., *Wu et al.*, 2006]. Here we use the TIDI Version 10 wind vector (VEC) data. These data have been used to study planetary-scale waves (tides) in this region [*Wu et al.*, 2008, 2009]. These studies employed the same *Wu et al.* [1995] analysis that will be used here. TIDI measures winds over almost the whole globe each day, with the measurements in the equatorial region coming from two local times, separated by ~12 hours. The slow precession rate of the satellite (~12 minutes/day) means that the local time difference between adjacent days' measurements is very small. This allows a study of even short-periods planetary waves from the TIDI observations.

[10] Following the launch of the TIMED satellite in 2002, the TIDI instrument faced some issues with its data quality due to ice on the optics of the instrument. These issues improved following two roll maneuvers of the spacecraft in 2003 and the gradual sublimation of this ice over time [*Skinner et al.*, 2003]. The data taken since 2005 are of improved quality [e.g., *Wu et al.*, 2008], but some data quality issues persist (data flagged as low quality in the TIDI Version 10 wind vector data) and thus some discussion of the quality of the TIDI data and how these are addressed in the present study is warranted.

[11] First, in order to use only the highest quality TIDI data, the data flagged as low quality are not used. Further, locations and times at which a significant number of such low-quality data points exist (see, for example, those marked in Figure 6) will be avoided wherever possible. As the TIDI wind observations are made using the $O_2^1\sigma$ (0–0) atmospheric band which peaks in brightness around 94 km altitude, the most detailed analysis of the TIDI data will be confined to the altitude bins closest to this.

[12] The precision of the TIDI observations must also be taken into consideration. These have been found from the photon counting statistics of the TIDI instrument and presented by *Wu et al.* [2008]. This study showed the precision of the observations as functions of altitude, latitude and time from 2002–2007. This study showed that the precision of the instrument improved with time from 2002–2005 and was essentially constant thereafter. Assuming the same precision values are representative of the TIDI data taken in 2010, considering the number of data points used and that a minimum of 4 unique samples are required to describe a sin wave, for the 9-day window that is used in much of the following analysis, the precision of the TIDI instrument limits the detection of 3-day waves to those with wind amplitudes above ~7 ms^{-1}. This applies to the results shown in Figures 5 and 9.

[13] Additionally, for the wavelet and Lomb-Scargle periodogram analyses that are presented, it is possible to compare the signals found to the total variance in the data and determine a statistical confidence level for each signal. This is used as an independent check of the validity of wave signatures identified in the TIDI wind observations (Figure 3).

2.4. Temperature Measurements Made by TIMED-SABER

[14] The Sounding of the Atmosphere using Broadband Emission Radiometry (SABER) instrument on TIMED has measured the neutral temperatures at various altitudes in the range of ~10–120 km since 2002 [*Remsberg et al.*, 2003]. The Level 2 kinetic temperature data (v1.07) are used in this study. These are available on a regularly spaced 2.5° × 2.5° latitude-longitude grid. These data (and previous versions) have been used to study tides [e.g., *Zhang et al.*, 2006; *Forbes et al.*, 2006] and planetary waves [e.g., *Pedatella and Forbes*, 2009; *Pancheva et al.*, 2010] in the MLT region. SABER has a similar spatial/temporal sampling to TIDI, allowing it to observe even short-period planetary waves [e.g., *Palo et al.*, 2007; *Forbes et al.*, 2009; *Chang et al.*, 2011].

3. Observations of the 3-Day Wave During January 2010

[15] Ground-based meteor and MF radars at low latitudes are an excellent means of determining the presence of equatorial planetary-scale waves in the mesosphere and have been used in numerous previous studies [*Riggin et al.*, 1997; *Kovalam et al.*, 1999; *Pancheva et al.*, 2004; *Younger and Mitchell*, 2006; *Davis et al.*, 2011]. Here we use data from the meteor radar at Thumba, India (8.5°N, 77°E) [*Kumar et al.*, 2007]. Figure 1 shows a wavelet plot of the zonal winds measured at 98 km altitude during January 2010 (data from December 1st 2009–February 28th 2010 are used to avoid windowing effects). While there is evidence of a longer-period wave (~6 days) present during first half of the month, the dominant short-period planetary wave observed has a period of around 3 days. This wave appears sporadically, with the strongest amplitudes observed in early January (~8th–12th) and again during the last third of the month (~20th–31st), both of which are statistically significant at the 85% level.

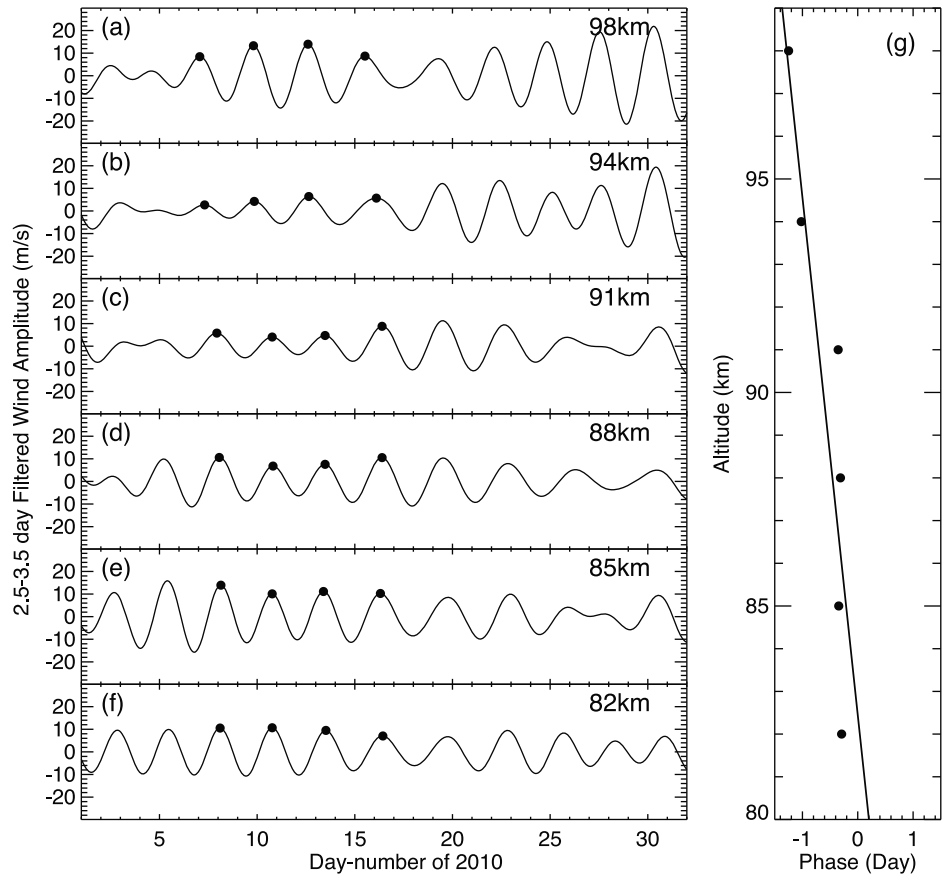

Figure 2. (a–f) Amplitude of 2.5–3.5 day filtered zonal winds measured by the SKiYMET radar at Thumba for 82–98 km altitudes over January 1–31, 2010. The dots mark the maxima of the winds. (g) Phase of the 3-day wave at different altitudes. The straight line is from the linear regression. The slope of the line indicates the vertical wavelength of this wave to be 30–40 km, assuming uncertainties for the period and least-squares fit.

[16] Using the data from the Thumba meteor radar, it is also possible to identify the vertical wavelength of this 3-day wave. Figures 2a–2f show the zonal winds observed at 82–98 km altitude, filtered for 2.5–3.5 day signatures. Using the crests of the wave at each altitude (shown by the black dots), it is possible to find the progression of the wave's phase with altitude (shown in Figure 2g). From the slope of this line and the frequency of the wave, it is possible to find the vertical wavelength. The vertical wavelength is 30–40 km, with both uncertainties in the frequency and slope accounted for in determining the uncertainty in the vertical wavelength.

[17] The 3-day period observed in the zonal winds at Thumba is indicative of an UFKW. To establish if this vertical wavelength is consistent with previous observations and theoretical calculations of UFKWs, it is necessary to also establish other properties of the wave, such as its horizontal wavelength (zonal wave number), which cannot be found from a single ground-based source. The TIDI instrument on TIMED [*Killeen et al.*, 2006; *Wu et al.*, 2006] is able to measure the horizontal winds in the MLT region. Unlike the observations from Thumba, TIMED is in a quasi-sun-synchronous orbit (precession rate ~12 minutes/day), allowing TIDI to make observations at all longitudes at a fixed local time (LT hereafter) in one day.

[18] To establish whether the same ~3-day signature is seen in the global-scale MLT region by TIDI, we select the data from 15th–31st January when the wave seen by Thumba is strongest. The periodicities in the zonal winds as a function of latitude at 87.5, 90.0 and 92.5 km altitude are shown in Figure 3. Three altitudes are shown to demonstrate the coherence of the wave signature across a range of altitudes. In this fixed LT frame, periods at and below 24 hours represent a combination of the longitudinal variations associated with wave such as non-migrating tides and day-to-day variations in the tides. The 3-day periodicity is prominent at equatorial latitudes at all three altitudes, with a maximum amplitude at the equator, dropping significantly by around $\pm 25°$, with a possible secondary signal around $-30°$ latitude. This prominent 3-day periodicity is strong at the latitude of Thumba (8.4°N), which suggests that both instruments may be observing the same wave.

[19] Having established the frequency of the wave observed by TIDI, it is possible to find the propagation direction (east or west) from these observations. Figure 4 shows the zonal winds observed by TIDI at equatorial latitudes as a function of longitude and time at 92.5 km altitude. The values at each longitude have been filtered for periods between 2.5–3.5 days to highlight the progression of the 3-day wave during the second half of January 2010,

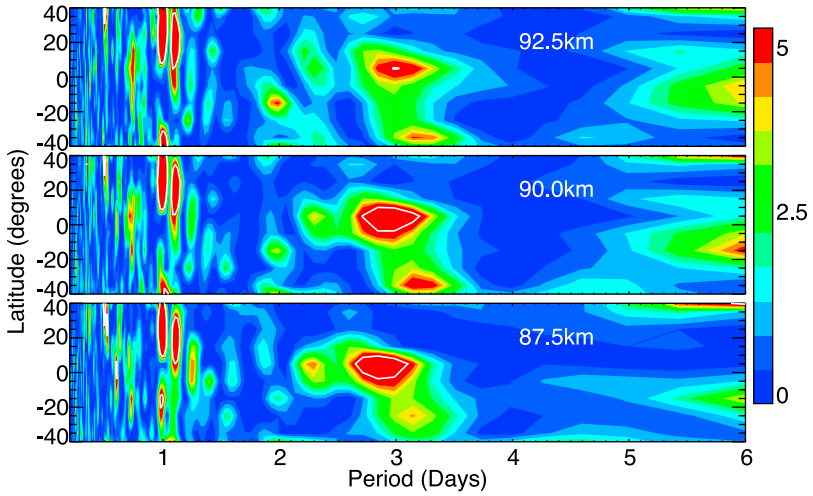

Figure 3. Lomb-Scargle normalized periodograms of the zonal winds measured by TIMED-TIDI at 87.5, 90.0 and 92.5 km altitude as a functions of latitude during January 17–31, 2010. The white contour lines mark the 85% statistical confidence level.

when the amplitude is greatest. Here, a strong 3-day wave with amplitude ~15 ms^{-1} is seen between days 20–30. The white dotted lines marked in Figure 4 show the phase progression of an eastward-propagating 3-day wave with a zonal wave number of 1. These show generally good agreement with the pattern in the zonal winds, indicating that this wave propagates eastward, consistent with an UFKW. Considering the winds as a function of longitude at a single point in time, this wave also appears to have a zonal wave number of 1, which is consistent with the most frequently observed 3-day UFKW described in section 1. However, there is some evidence that other zonal wave numbers may also be present (for example around day 23, when two maxima as a function of longitude are seen). As 3-day waves with wave numbers of 1, 2 and 3 have all previously been observed [e.g., *Lieberman and Riggin*, 1997], we employ the analysis method of *Wu et al.* [1995] to identify the amplitudes of the eastward-propagating wave number-1, -2 and -3 components of the 3-day wave. This analysis identifies the amplitude and phase of the wave assuming its period and zonal wave number are known. Here this analysis is applied to a 9-day running window of the TIDI data. These are shown as a function of time at 92.5 km altitude in Figure 5. This analysis shows that while some evidence for wave number-2 and -3 components is seen in the TIDI data, these two components are generally weak compared to the wave number-1 component and are mostly below the 7 ms^{-1} detection threshold described in section 2.3. Thus, we shall focus on the 3-day wave of zonal wave number-1 henceforth.

[20] Having established the phase speed of the wave, further examination of the wave's horizontal wind structure as a function of latitude is now possible. Figure 3 shows that the 3-day component of the zonal wind peaks close to the equator (slightly north) and is generally symmetric about the

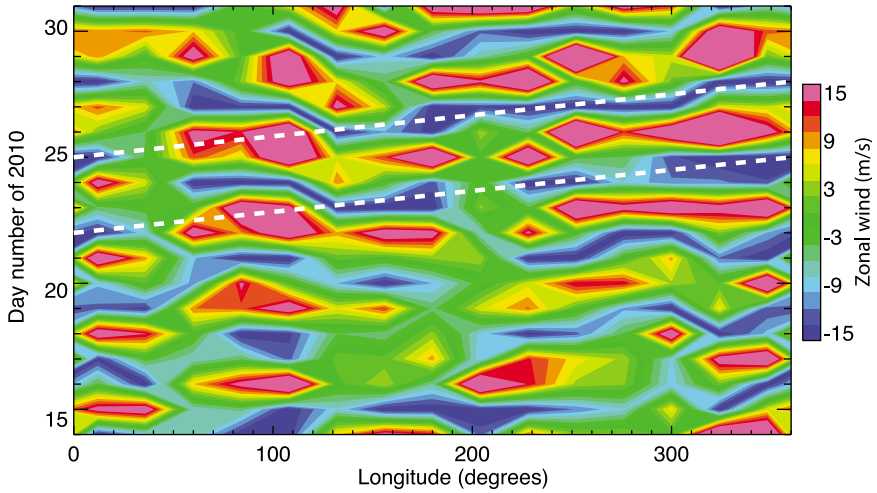

Figure 4. Zonal winds as a function of longitude and time from January 14–31 measured by TIMED-TIDI at 92.5 km altitude, averaged over ±10° latitude and filtered for 2.5–3.5 day periods. The dashed white line corresponds to eastward propagation at the rate of one equatorial circumference every 3 days.

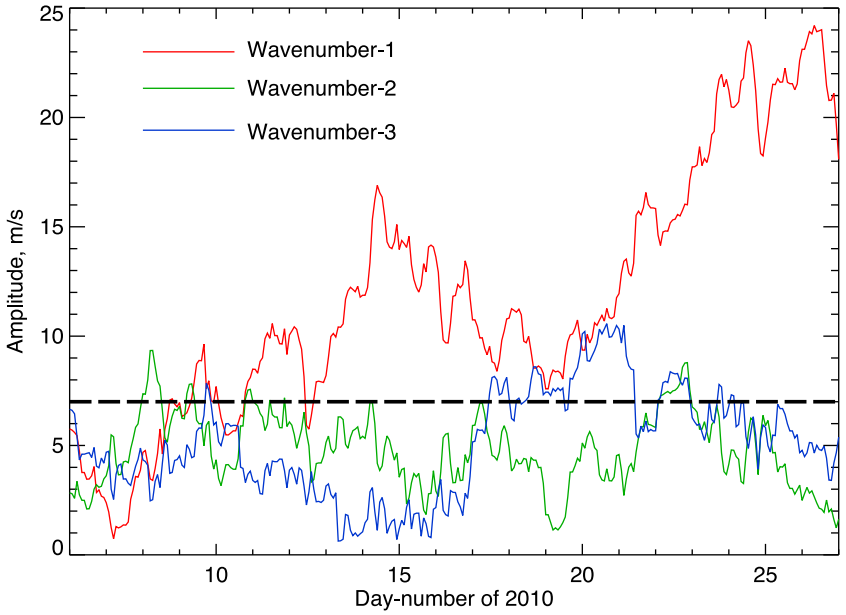

Figure 5. Amplitudes of the 3-day eastward wave numbers-1, -2 and 3 waves identified in the zonal winds observed by TIMED-TIDI at 92.5 km during January 2010. Values are shown represent the amplitude over a 9-day bin, centered on the time shown. The 7 ms^{-1} detectability threshold for the 3-day wave (section 2.3) is marked by the horizontal dashed line.

equator, which is as expected for an UFKW. These waves are trapped in the equatorial region and *Holton and Lindzen* [1968] showed that their latitudinal half-width is given by

$$L_y \simeq \sqrt{\frac{2\omega}{\beta k}} \quad (1)$$

where L_y is the latitudinal half-width, $\frac{\omega}{k}$ is the zonal phase speed (given by Figure 4) and $\beta = \frac{2\omega}{r_E}$ where ω is the rotation rate of the Earth and r_E is the radius of the Earth. This theoretical calculation gives the half-width of the 3-day UFKW to be ~30°. This is slightly larger than that suggested by Figure 3, which is ~25°, but the observations confirm that the wave is trapped in the equatorial region with an

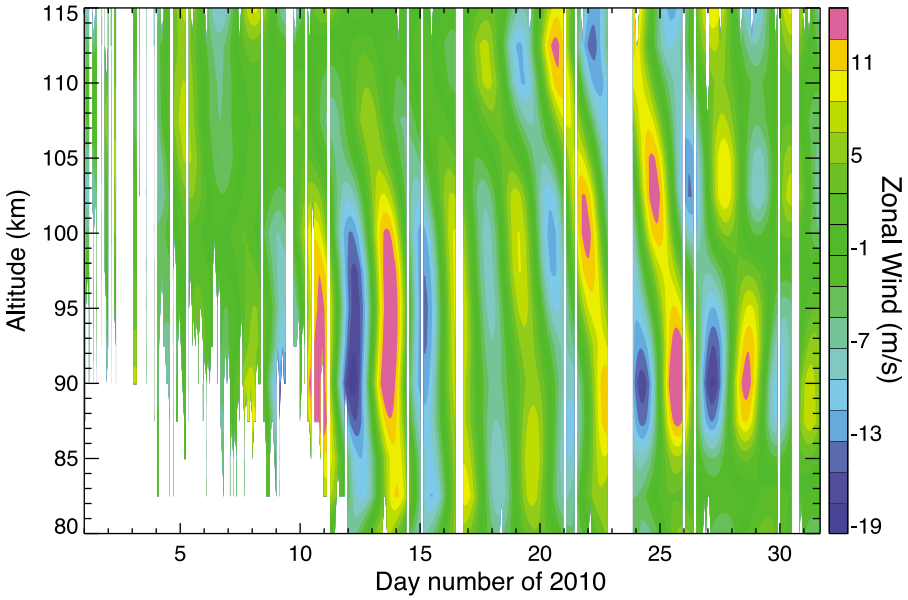

Figure 6. Altitude-time reconstruction of the 3-day eastward wave number-1 component of the zonal winds measured by TIMED-TIDI over ±10° latitude throughout January 2010. The downward phase propagation of this wave as a function of time can be seen. Using the clear phase propagation between days 17–29, the vertical wavelength is estimated to be ~40 km. Periods of low-quality or missing data are marked in white.

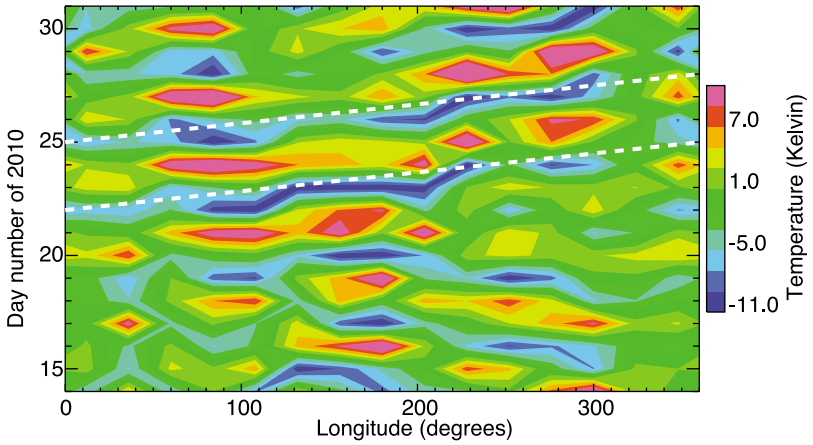

Figure 7. As Figure 4, but for the temperatures measured by TIMED-SABER, averaged over 0–20° latitude.

amplitude that decays with latitude, which is consistent with the theoretical description of an UFKW.

[21] Having demonstrated the frequency, wave number and propagation direction of the 3-day wave, we again employ the analysis method of *Wu et al.* [1995] to identify the wave number-1 component in the TIDI data. Figure 6 shows the reconstruction of this wave analysis for the zonal winds averaged over ±10° latitude as a function of altitude from 80–115 km throughout January 2010. The TIDI data set includes a few data gaps, especially in the first 10 days of the month, which are marked in white. The 3-day wave is seen at significant amplitude around days 10–15 and 20–30, which is in general agreement with the Thumba observations. As in the Thumba observations shown in Figure 2, the phase of the wave propagates downward with time, which is consistent with an upward propagating UFKW. Using days 20–30, the vertical wavelength is estimated to be ∼40 km, which is again in overall agreement with the Thumba observations. Thus, we can be confident that both instruments are observing the same wave. As TIDI is able to measure the zonal wind up to ∼115 km, albeit with decreased precision as the atmospheric emissions used by TIDI to measure the neutral winds (from O_2 and O) drop rapidly in brightness above 100 km, it can be seen from these observations that the wave propagates to ∼100–105 km, above which its amplitude drops with altitude. This indicates that the 3-day wave propagates into the lower thermosphere, as has been previously reported for the UFKW [*Lieberman and Riggin*, 1997; *Forbes et al.*, 2009].

[22] Having established the observed vertical wavelength of the 3-day wave at equatorial latitudes, it is instructive to compare this with previous observations and theoretical calculations of the UFKW. From the Kelvin wave dispersion relation [e.g., *Holton et al.*, 2001].

$$\lambda_z = N\left[\frac{\lambda_x}{\tau} - \overline{u}\right] \quad (2)$$

where λ_z is the vertical wavelength, N is the Brunt-V*äisälä* period, τ is the wave period and $\overline{u}$ is the zonal mean zonal wind, if we use typical values for $N \simeq 300$ s and taking a typical value of $\overline{u}$ as 20 ms^{-1} for January at 90 km altitude (the middle of our observed altitude range from TIDI) from the UARS Reference Atmosphere Project [*Swinbank and Ortland*, 2003], we find that the vertical wavelength of a 3-day wave number-1 Kelvin wave is expected to be ∼41 km. This is in good agreement with the value found from both the Thumba and TIDI observations and is also consistent with several previous observations of the UFKW [*Salby et al.*, 1984; *Sridharan et al.*, 2002; *Davis et al.*, 2011]. This, combined with the wave period and eastward propagation provides strong evidence that the wave observed at equatorial latitudes during January 2010 is an UFKW.

[23] The temperature structure of the 3-day wave can be explored using data from the TIMED-SABER instrument. SABER measures the temperature in the MLT region in a quasi-fixed LT frame similar to that of TIDI, but unlike TIDI, SABER had an ∼100% duty cycle during January 2010. Using the SABER data, it is possible to repeat the same analysis as was shown for TIDI. Two instructive examples using the SABER data are shown in Figures 7 and 8 that correspond to the TIDI analyses shown in Figures 4 and 6. Figure 7 confirms the presence of a clear 3-day, eastward propagating wave in the second half of January 2010. In the SABER data, this wave is particularly clear around days 21–30, which is in general agreement with the two sets of wind observations shown above. Figure 8 confirms that the wave propagates with increasing amplitude up to ∼105 km, above which it begins to dissipate. The correspondence between Figures 4 and 8 is not perfect, especially above 100 km. For example, the largest amplitudes observed by TIDI above 110 km occur on days 19–23, whereas the largest amplitudes observed by SABER at these altitudes occur around days 9–13. Such a disagreement may be expected as neither instrument performs optimally at these altitudes.

[24] For a closer examination of the correspondence between the observations from SABER and TIDI, it is instructive to compare the signature of the 3-day wave in the geopotential heights derived from SABER observations and the horizontal winds observed by TIDI. For this, we perform the same analysis to identify the 3-day eastward propagating

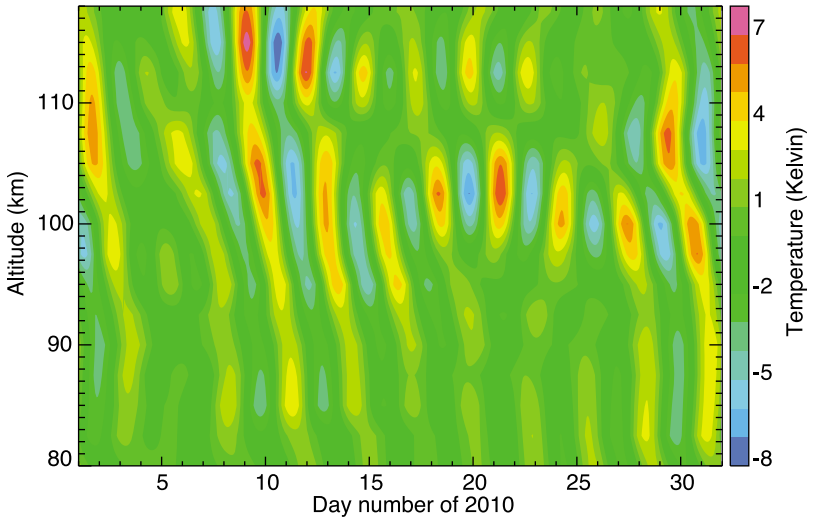

Figure 8. As Figure 6, but for the temperatures measured by TIMED-SABER, averaged over 0–20° latitude.

wave number-1 signature (following *Wu et al.* [1995]) in the geopotential heights, zonal and meridional winds across a range of latitudes. This analysis is performed for the winds at 95 km altitude (close to the peak of the O_2 airglow at 94 km) and a corresponding pressure level of 5×10^{-4} mbar using the observations from 13th–21st January (which overlaps with the Arecibo data shown below). A reconstruction of the wave found in each of these fields is shown in Figure 9. At the lowest latitudes (below ~15°), a peak in the geopotential that is symmetrical about the equator is seen. The winds in this region are primarily zonal, moving eastward in regions of high geopotential and westward in regions of low geopotential. This provides strong evidence for the existence of a Kelvin wave at these latitudes [e.g., *Andrews et al.*, 1987]. At higher latitudes (~30–40°) an anti-symmetric pattern is seen in the geopotential field and the associated winds have both meridional and zonal components that are anti-symmetric about the equator, which is indicative of a higher-order equatorial mode such as a Rossby-gravity wave [e.g., *Andrews et al.*, 1987]. At intermediate latitudes (~20°), both the geopotential and wind fields show a mixture of the contributions from these two modes of the 3-day wave. For completeness, the wave number-2 and -3 components were also examined in the same manner (not shown here), but the horizontal wind components associated with these were below the detectability threshold of TIDI during this time period (see Figure 5).

[25] To examine the signature of the UFKW above 100 km, an excellent alternative to the meteor radar and TIMED data shown above is the high-power ISR at Arecibo, Puerto Rico (18°N, 66°W). From the 14th–23rd January 2010, the Arecibo ISR was operating continuously as part of

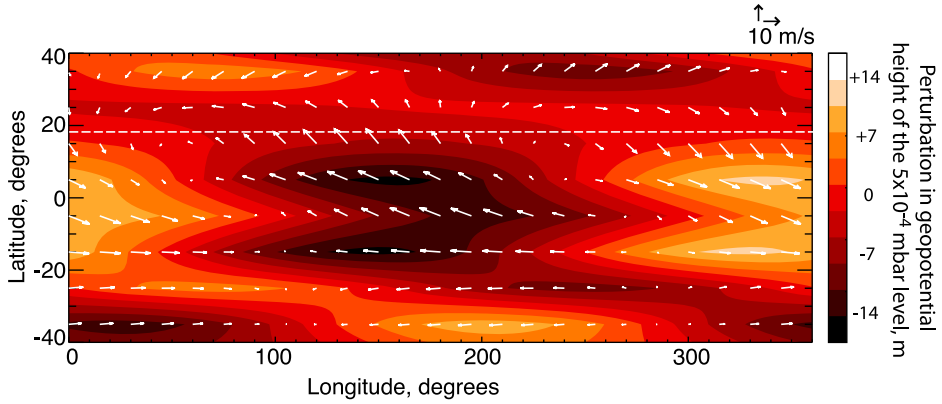

Figure 9. Latitude-longitude reconstruction of the geopotential height (contours) and horizontal wind (vectors) fluctuations associated with the 3-day eastward wave number-1 wave observed by TIMED-SABER (geopotential heights) and -TIDI (winds). The wave-component of the winds at 95 km altitude and the geopotential height of the 5×10^{-4} mbar surface for January 13th–21st 2010 are shown. The reconstruction corresponds to a universal time of 0 hours. The white dashed line shows the latitude of the Arecibo ISR.

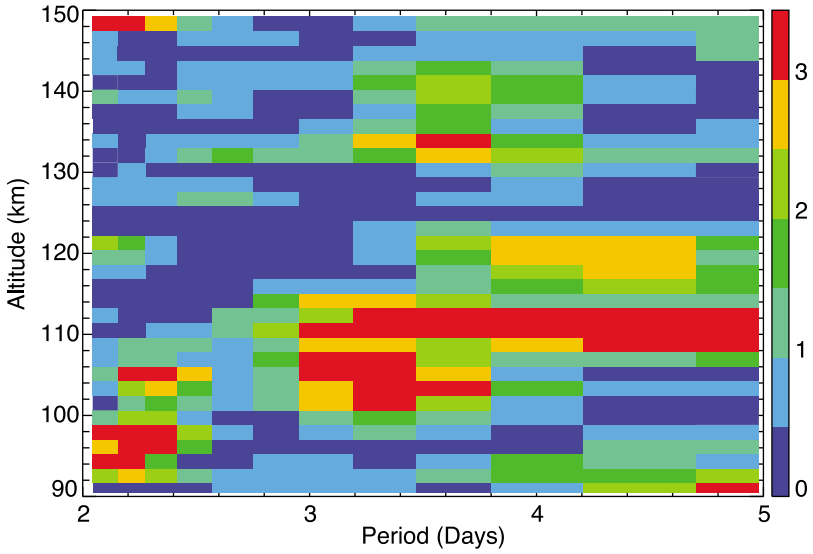

Figure 10. Lomb-Scargle normalized periodogram of the meridional winds as a function of altitude measured by the Arecibo ISR from 14th–23rd January 2010.

the International Union of Radio Science (URSI) World Day campaign to observe the atmospheric and ionospheric impacts of SSW. The continuous observations by the Arecibo ISR during this period offers a rare opportunity to study a 3-day wave with this kind of facility. Indeed, to our knowledge, the results shown below are the first published observations of a 3-day wave with any ISR.

[26] Examining the wind pattern shown in Figure 9, both zonal and meridional winds associated with the combination of the two 3-day wave modes should be present at the latitude of Arecibo (marked in Figure 9) of which the ISR is only able to measure the meridional component well (see section 2.2). Here we employ the analysis method of *Zhou et al.* [1997a] to find the periodic signatures in these winds. Figure 10 shows a periodogram of the meridional winds as a function of altitude. As discussed in section 2.2, we employ the coherence of determined signatures between adjacent altitude bins as an indicator of confidence in the observed signatures. While not as dominant as the signature seen by TIDI (Figure 3), a significant 3–3.5 day signature is seen between 100–115 km altitude. Assuming therefore that the signature seen in the Arecibo observations is that of the same 3-day wave at intermediate latitudes described above, we see that during this period, the 3-day wave does not propagate above ~115 km altitude with any detectable amplitude. This is in agreement with the behavior of the 3-day wave observed by *Lieberman and Riggin* [1997] and *Forbes et al.* [2009].

[27] At altitudes up to ~150 km, where the ion-neutral frequency is high, the ion temperatures are close to the neutral temperatures, which allows us to use these as an indicator of periodicities in the neutral atmosphere. As this proxy relies upon a high ion-neutral frequency, this altitude range also coincides with that of the E-region dynamo [*Kato*, 1956, 1957], which can be significantly impacted by a 3-day wave [*Takahashi et al.*, 2006, 2007; *Chang et al.*, 2010]. An analysis of the ion temperature observations made by Arecibo, similar to that for the meridional winds shown in Figure 10 was performed, but no evidence of the 3-day wave was found. While this is no conclusive, it is consistent with the interpretation that the 3-day wave does not propagate at significant amplitude above ~115 km.

4. Evidence of the Interaction of the 3-Day Wave With the Diurnal Tide

[28] The vertical wavelength of the UFKW observed at low latitudes during January 2010 is close to that of several of the highest amplitude tides in the equatorial MLT region (e.g. the diurnal migrating tide and the non-migrating eastward propagating diurnal wave number 2 and 3 tides) and thus it may be expected that this wave could interact strongly with these tides. *Teitelbaum and Vial* [1991] proposed that such non-linear interactions between planetary waves and tides can result in the generation of two 'child-waves', whose periods and wave numbers are the sums and differences of the two parent waves. Such child-waves then produce a modulation of the tide with the period of the parent planetary wave. As it is generally believed that most planetary-waves cannot propagate into the thermosphere, whereas many tides can, this mechanism has been proposed as one pathway by which planetary-wave signatures can be communicated to the ionosphere [e.g., *Pancheva et al.*, 2002, 2006]. For the specific case of the 3-day wave, the picture is less clear. A recent study by *Chang et al.* [2010] simulated the generation of child-waves by the 3-day wave in the TIME-GCM model, but the 3-day wave was also seen to propagate to ionospheric dynamo region in their model. For the case of January 2010, the 3-day wave is not seen to propagate with significant amplitude into the dynamo region and thus any interaction between the 3-day wave and tides may be important for the understanding the potential influence of this wave on the day-to-day variations in the ionosphere around this time.

[29] Figure 11 shows a periodogram of the diurnal tidal amplitudes at Thumba at 82, 88 and 98 km altitudes (as measured by their meridional wind components which are strong at Thumba). A significant 3-day modulation of the amplitude of the diurnal tide is seen around days 15–25

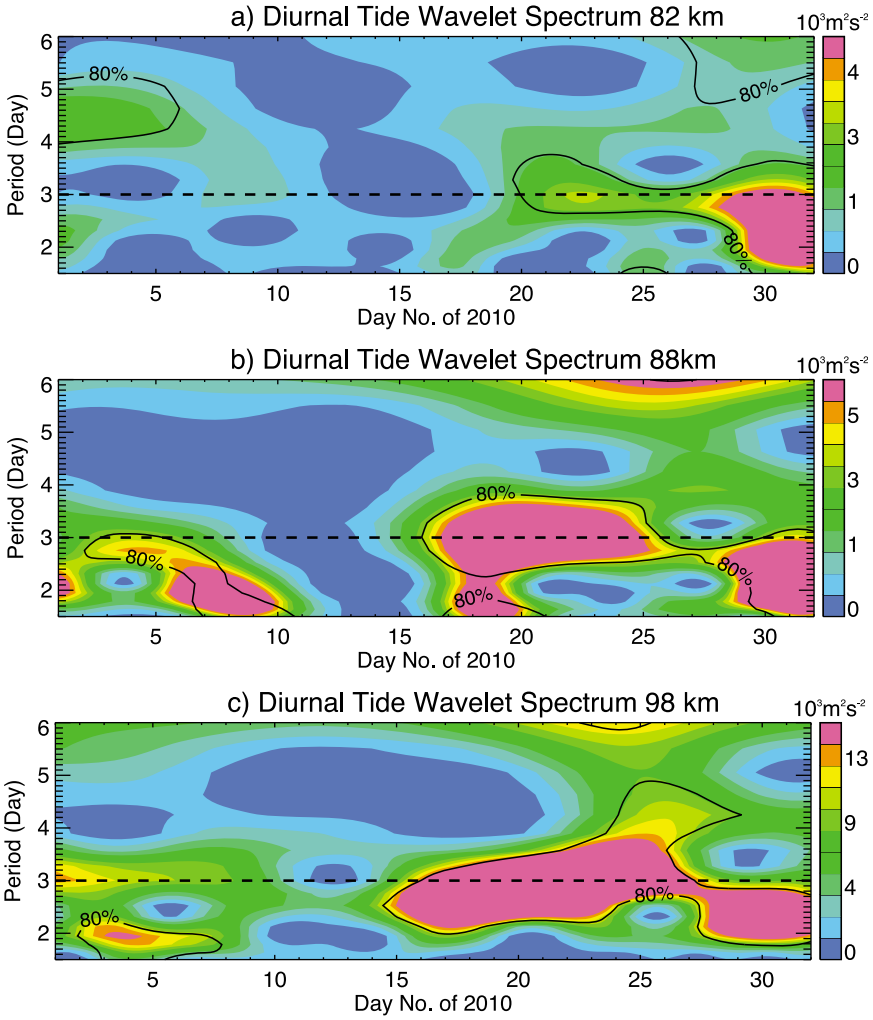

Figure 11. Wavelet plots of the diurnal tidal amplitude as a function of time and period throughout January 2010 measured in the meridional wind observations form the meteor radar at Thumba at (a) 82, (b) 88 and (c) 98 km altitude. Note, data from December 1, 2009 to February 28, 2010 were used in the analysis to avoid wavelet edge effects.

at 88 and 98 km (at the 80% confidence level), but not seen at the lower altitude (82 km). This suggests that a non-linear interaction between the diurnal tide and the 3-day wave occurs during this time period and that his interaction may occur in the 82–88 km altitude range. The amplitude of the 3-day tidal modulation is larger at 98 km than 88 km, which suggest that the child-waves produced grow with altitude and may propagate into the thermosphere as simulated by *Chang et al.* [2010].

[30] Using the observations from Thumba, it is also possible to directly detect the child-waves produced from this interaction. Figure 12 shows periodograms of the zonal and meridional winds at 98 km, using data from 15th–31st January (where the strongest modulation of the 3-day wave is seen by Thumba). As may be expected, the diurnal and semi-diurnal tides can be seen in both wind components and the 3-day wave is seen only in the zonal component at Thumba. The blue and red lines marked on the figure show the frequencies that correspond to the two child-waves that would be produced from the non-linear interaction of the 3-day wave with the diurnal and semi-diurnal tides, respectively. Of the two expected child-waves associated with the diurnal tide, only the wave with a period of 36 hours is seen at Thumba. This wave is strongest in the meridional component, but is present in both zonal and meridional components at the 80% confidence level. It is not clear why no corresponding wave with a period of 18 hours is seen, but similar behavior has been reported in an analyses by *Moudden and Forbes* [2010]. No clear evidence of any child-waves associated with the semi-diurnal tide can be seen, suggesting that the non-linear interaction occurs only between the 3-day wave and the diurnal tide.

[31] *Zhou et al.* [1997a] demonstrated that the Arecibo ISR can observe the meridional wind signature associated with the diurnal tide up to an altitude of ~150 km with good height resolution. The observations from Arecibo (days 14–23) overlap well with the 3-day modulation of the diurnal tide observed at Thumba (days 15–25), and both the child-wave and modulation of the tide are observed most strongly in the meridional wind component at Thumba, therefore the Arecibo ISR may offer an ideal way to further explore the modulation of the diurnal tide at thermospheric altitudes.

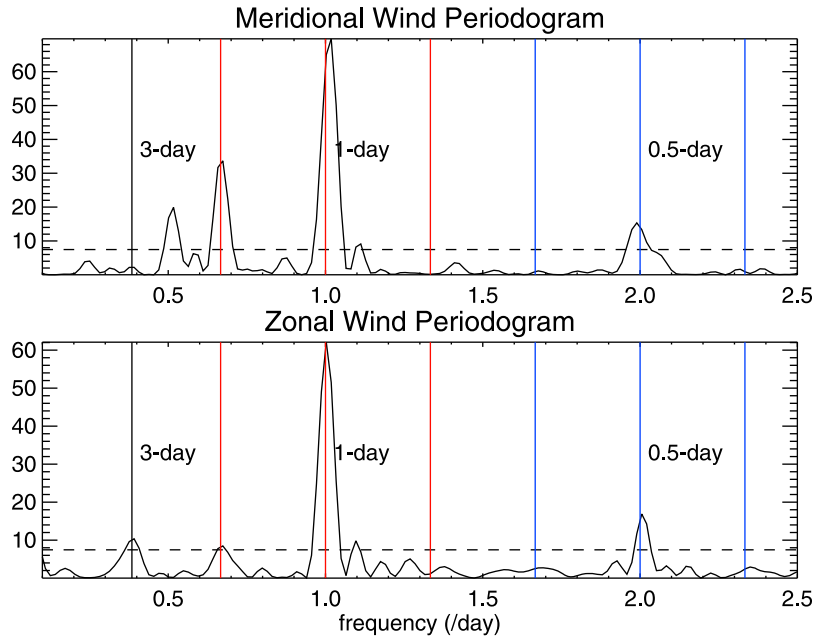

Figure 12. Lomb-Scargle normalized periodograms of the (top) meridional and (bottom) zonal winds observed by the meteor radar at Thumba at 98 km altitude during January 15th–31st 2010. The vertical black line marks the frequency of the 3-day wave, the red lines show the frequencies of the diurnal tide and its two associated child-waves and the blue lines mark the frequencies of the semi-diurnal tide and its two associated child-waves, each assuming a non-linear interaction with the 3-day wave. The horizontal dashed lines mark the 80% confidence level.

Figure 13 shows a periodogram of the amplitude of the diurnal tide (as measured by the meridional winds) observed by Arecibo as a function of altitude. A clear 3-day modulation of the diurnal amplitudes is seen continuously across the altitude range of ∼115–145 km. This, along with the observations in the MLT region by the meteor radar at Thumba, suggest that a non-linear interaction between the 3-day wave and the diurnal tide occurs in the mesosphere between 82 and 89 km and at least one of the resultant child-waves propagate up to ∼145 km. As the 3-day wave observed here does not propagate with significant amplitude up to the altitude of the ionospheric dynamo region, but the 3-day modulation of the diurnal tide is strong throughout the highly conducting E-region, it may be possible for the 3-day wave to indirectly influence the ionosphere via the child-waves described here.

[32] In a recent study, *H.-L. Liu et al.* [2010c] used the TIME-GCM model to study the non-linear interaction

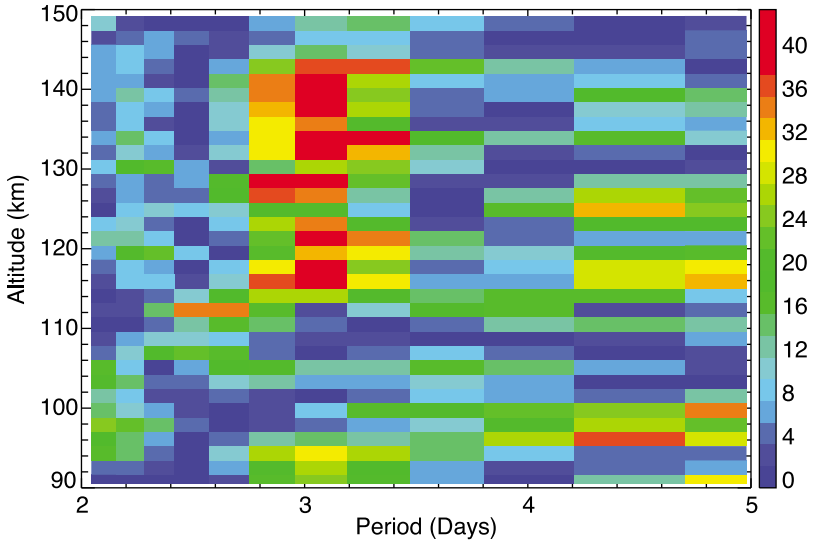

Figure 13. As Figure 10, but for the diurnal-tidal amplitudes measured from the meridional winds observed by the Arecibo ISR.

between planetary waves and tides and the subsequent impact on the E-region dynamo. They showed that, even though the planetary waves simulated in their model did not directly impact the E-region, the non-linear interaction with tides allowed them to indirectly produce a significant day-to-day modulation of the dynamo. Further, this study showed that as tides are global in nature, the planetary wave–tide interaction provided a means for communicating the planetary wave signature across a wide range of latitudes (from high to equatorial latitudes in the case studied by *H.-L. Liu et al.* [2010c]. Thus, for the case of January 2010, where the 3-day wave is confined to relatively low latitudes (e.g. Figure 3), it may be possible for this wave to indirectly impact the ionosphere at higher latitudes via the non-linear interaction identified here. A detailed study of the impact of this wave on the ionosphere is beyond the scope of the present work. *Liu et al.* [2012] present evidence of a clear 3-day ionospheric modulation at low latitudes and midlatitudes that the authors demonstrate is related to the wave described here.

5. Conclusions

[33] 1. A 3-day equatorial wave is observed in the mesosphere and lower thermosphere during January 2010. The wave is seen to propagate eastward, has a zonal wave number of 1 and a vertical wavelength of ∼40 km.

[34] 2. The 3-day wave is identified in a variety of observations, both from the ground and space, including the first ever observations of a 3-day wave with an ISR.

[35] 3. At the lowest latitudes (below ∼15°) the geopotential and wind oscillations associated with the 3-day wave show a clear Kelvin mode pattern. At higher latitudes (∼30–40°), these fields are indicative of a Rossby-gravity wave mode. At intermediate latitudes (∼20°), the geopotential and wind fields appear to be a mixture of these two modes.

[36] 4. For the case of studied here, the 3-day wave is seen to propagate directly to ∼105 km altitude.

[37] 5. Evidence of a non-linear interaction with the diurnal tide is seen with the ground-based meteor radar at Thumba and ISR at Arecibo. This interaction appears to occurs in the 82–88 km altitude region and the child-waves produced from this propagate up through the altitude range of the E-region ionosphere (to ∼150 km altitude).

[38] **Acknowledgments.** This work was supported by the National Science Foundation's CEDAR program through Award numbers AGS-1042261 and AGS-1042223 and the National Aeronautics and Space Administration's Heliophysics Research program through Award number NNX12AD48G. The Arecibo Observatory is operated by SRI International under a cooperative agreement with the National Science Foundation (AST-1100968), in an alliance with Ana G. Méndez-Universidad Metropolitana, and the Universities Space Research Association.

[39] Robert Lysak thanks the reviewers for their assistance in evaluating this paper.

References

Andrews, D. A., J. R. Holton, and C. B. Leovy (1987), *Middle Atmosphere Dynamics*, pp. 202–206, Academic, San Diego, Calif.

Aponte, N., M. J. Nicolls, S. A. González, M. P. Sulzer, M. C. Kelley, E. Robles, and C. A. Tepley (2005), Instantaneous electric field measurements and derived neutral winds at Arecibo, *Geophys. Res. Lett.*, *32*, L12107, doi:10.1029/2005GL022609.

Bertoni, F. C. P., Y. Sahai, J.-P. Raulin, P. R. Fagundes, V. G. Pillat, C. G. Gimenez de Castro, and W. L. C. Lima (2011), Equatorial spread-F occurrence observed at two near equatorial stations in the Brazilian sector and its occurrence modulated by planetary waves, *J. Atmos. Sol. Terr. Phys.*, *73*, 457–463, doi:10.1016/j.jastp.2010.10.017.

Chang, L. C., S. E. Palo, H.-L. Liu, T.-W. Fang, and C. S. Lin (2010), Response of the thermosphere and ionosphere to an ultra fast Kelvin wave, *J. Geophys. Res.*, *115*, A00G04, doi:10.1029/2010JA015453.

Chang, L. C., J.-Y. Liu, and S. E. Palo (2011), Propagating planetary wave coupling in SABER MLT temperatures and GPS TEC during the 2005/2006 austral summer, *J. Geophys. Res.*, *116*, A10324, doi:10.1029/2011JA016687.

Chau, J. L., L. P. Goncharenko, B. G. Fejer, and H.-L. Liu (2012), Equatorial and low latitude ionospheric effects during sudden stratospheric warming events, *Space Sci. Rev.*, doi:10.1007/s11214-011-9797-5, in press.

Davis, R. N., Y.-W. Chen, S. Miyahara, and N. J. Mitchell (2011), The climatology, propagation and excitation of ultra-fast Kelvin waves as observed by meteor radar, Aura MLS, TRMM and in the Kyushu-GCM, *Atmos. Chem. Phys. Disc.*, *11*, 29,479–29,525, doi:10.5194/acpd-11-29479-2011.

England, S. L. (2012), A Review of the Effects of Non-migrating Atmospheric Tides on the Earth's Low-Latitude Ionosphere, *Space Sci. Rev.*, doi:10.1007/s11214-011-9842-4, in press.

Fagundes, P. R., V. G. Pillat, M. J. A. Bolzan, Y. Sahai, F. Becker-Guedes, J. R. Abalde, S. L. Aranha, and J. A. Bittencourt (2005), Observations of F layer electron density profiles modulated by planetary wave type oscillations in the equatorial ionospheric anomaly region, *J. Geophys. Res.*, *110*, A12302, doi:10.1029/2005JA011115.

Fagundes, P. R., J. R. Abalde, J. A. Bittencourt, Y. Sahai, R. G. Francisco, V. G. Pillat, and W. L. C. Lima (2009a), F layer postsunset height rise due to electric field prereversal enhancement: 2. Traveling planetary wave ionospheric disturbances and their role on the generation of equatorial spread F, *J. Geophys. Res.*, *114*, A12322, doi:10.1029/2009JA014482.

Fagundes, P. R., J. A. Bittencourt, J. R. Abalde, Y. Sahai, M. J. A. Bolzan, V. G. Pillat, and W. L. C. Lima (2009b), F layer postsunset height rise due to electric field prereversal enhancement: 1. Traveling planetary wave ionospheric disturbance effects, *J. Geophys. Res.*, *114*, A12321, doi:10.1029/2009JA014390.

Forbes, J. M. (2000), Wave coupling between the lower and upper atmosphere: case study of an ultra-fast Kelvin wave, *J. Atmos. Sol. Terr. Phys.*, *62*, 1603–1621, doi:10.1016/S1364-6826(00)00115-2.

Forbes, J. M., J. Russell, S. Miyahara, X. Zhang, S. Palo, M. Mlynczak, C. J. Mertens, and M. E. Hagan (2006), Troposphere-thermosphere tidal coupling as measured by the SABER instrument on TIMED during July-September 2002, *J. Geophys. Res.*, *111*, A10S06, doi:10.1029/2005JA011492.

Forbes, J. M., X. Zhang, S. E. Palo, J. Russell, C. J. Mertens, and M. Mlynczak (2009), Kelvin waves in stratosphere, mesosphere and lower thermosphere temperatures as observed by TIMED/SABER during 2002–2006, *Earth Planets Space*, *61*, 447–453.

Goncharenko, L., and S.-R. Zhang (2008), Ionospheric signatures of sudden stratospheric warming: Ion temperature at middle latitude, *Geophys. Res. Lett.*, *35*, L21103, doi:10.1029/2008GL035684.

Hedin, A. E. (1992), MSISE model (1990), *Planet. Space Sci.*, *40*, 556, doi:10.1016/0032-0633(92)90210-F.

Hirota, I. (1979), Kelvin waves in the equatorial middle atmosphere observed by the Nimbus 5. SCR., *J. Atmos. Sci.*, *36*, 217–222, doi:10.1175/1520-0469(1979)036<0217:KWITEM>2.0.CO;2.

Holton, J. R. (1973), On the frequency distribution of atmospheric Kelvin waves, *J. Atmos. Sci.*, *30*, 499–500, doi:10.1175/1520-0469(1973)030<0499:OTFDOA>2.0.CO;2.

Holton, J. R., and R. S. Lindzen (1968), A note on "Kelvin" waves in the atmosphere, *Monthly Weather Rev.*, *96*, 385–386, doi:10.1175/1520-0493(1968)096<0385:ANOKWI>2.0.CO;2.

Holton, J. R., M. J. Alexander, and M. T. Boehm (2001), Evidence for short vertical wavelength Kelvin waves in the department of energy-atmospheric radiation measurement Nauru99 radiosonde data, *J. Geophys. Res.*, *106*, 20,125–20,130, doi:10.1029/2001JD900108.

Isham, B., C. A. Tepley, M. P. Sulzer, Q. H. Zhou, M. C. Kelley, J. S. Friedman, and S. A. González (2000), Upper atmospheric observations at the Arecibo Observatory: Examples obtained using new capabilities, *J. Geophys. Res.*, *105*, 18,609–18,638, doi:10.1029/1999JA900315.

Kato, S. (1956), Horizontal wind-systems in the ionospheric E region deduced from the dynamo theory of the geomagnetic S_q variation. Part II. Rotating Earth, *J. Geomagn. Geolectr.*, *8*, 24–37.

Kato, S. (1957), Horizontal wind-systems in the ionospheric E region deduced from the dynamo theory of the geomagnetic S_q variation. Part IV., *J. Geomagn. Geolectr.*, *9*, 107–115.

Killeen, T. L., Q. Wu, S. C. Solomon, D. A. Ortland, W. R. Skinner, R. J. Niciejewski, and D. A. Gell (2006), TIMED Doppler Interferometer: Overview and recent results, *J. Geophys. Res.*, *111*, A10S01, doi:10.1029/2005JA011484.

Kovalam, S., R. A. Vincent, I. M. Reid, T. Tsuda, T. Nakamura, K. Ohnishi, A. Nuryanto, and H. Wiryosumarto (1999), Longitudinal variations in planetary wave activity in the equatorial mesosphere, *Earth Planets Space*, *51*, 665–674.

Kumar, K. K., G. Ramkumar, and S. T. Shelbi (2007), Initial results from SKiYMET meteor radar at Thumba (8.5°N, 77°E): 1. Comparison of wind measurements with MF spaced antenna radar system, *Radio Sci.*, *42*, RS6008, doi:10.1029/2006RS003551.

Lieberman, R. S., and D. Riggin (1997), High resolution doppler imager observations of Kelvin waves in the equatorial mesosphere and lower thermosphere, *J. Geophys. Res.*, *102*, 26,117–26,130, doi:10.1029/96JD02902.

Liu, G., T. J. Immel, S. L. England, K. K. Kumar, and G. Ramkumar (2010a), Temporal modulations of the longitudinal structure in F_2 peak height in the equatorial ionosphere as observed by COSMIC, *J. Geophys. Res.*, *115*, A04303, doi:10.1029/2009JA014829.

Liu, G., T. J. Immel, S. L. England, K. K. Kumar, and G. Ramkumar (2010b), Temporal modulation of the four-peaked longitudinal structure of the equatorial ionosphere by the 2 day planetary wave, *J. Geophys. Res.*, *115*, A12338, doi:10.1029/2010JA016071.

Liu, G., S. L. England, T. J. Immel, K. K. Kumar, G. Ramkumar, and L. Goncharenko (2012), Signatures of the 3-day wave in the low- and mid-latitude ionosphere during the January 2010 URSI World Day campaign, submitted, *J. Geophys. Res.*, doi:10.1029/2012JA017588, in press.

Liu, H.-L., W. Wang, A. D. Richmond, and R. G. Roble (2010c), Ionospheric variability due to planetary waves and tides for solar minimum conditions, *J. Geophys. Res.*, *115*, A00G01, doi:10.1029/2009JA015188.

Moudden, Y., and J. M. Forbes (2010), A new interpretation of Mars aerobraking variability: Planetary wave-tide interactions, *J. Geophys. Res.*, *115*, E09005, doi:10.1029/2009JE003542.

Palo, S. E., J. M. Forbes, X. Zhang, J. M. Russell, and M. G. Mlynczak (2007), An eastward propagating two-day wave: Evidence for nonlinear planetary wave and tidal coupling in the mesosphere and lower thermosphere, *Geophys. Res. Lett.*, *34*, L07807, doi:10.1029/2006GL027728.

Pancheva, D., N. Mitchell, R. R. Clark, J. Drobjeva, and J. Lastovicka (2002), Variability in the maximum height of the ionospheric F2-layer over Millstone Hill (September 1998Â March 2000); influence from below and above, *Ann. Geophys.*, *20*, 1807–1819, doi:10.5194/angeo-20-1807-2002.

Pancheva, D., N. Mitchell, and P. Younger (2004), Meteor radar observations of atmospheric waves in the equatorial mesosphere/lower thermosphere over Ascension Island, *Ann. Geophys.*, *22*, 387–404, doi:10.5194/angeo-22-387-2004.

Pancheva, D. V., et al. (2006), Two-day wave coupling of the low-latitude atmosphere–ionosphere system, *J. Geophys. Res.*, *111*, A07313, doi:10.1029/2005JA011562.

Pancheva, D., P. Mukhtarov, B. Andonov, and J. M. Forbes (2010), Global distribution and climatological features of the 5-6-day planetary waves seen in the SABER/TIMED temperatures (2002–2007), *J. Atmos. Sol. Terr. Phys.*, *72*, 26–37, doi:10.1016/j.jastp.2009.10.005.

Pedatella, N. M., and J. M. Forbes (2009), Modulation of the equatorial F-region by the quasi-16-day planetary wave, *Geophys. Res. Lett.*, *36*, L09105, doi:10.1029/2009GL037809.

Pogoreltsev, A. I., A. A. Vlasov, K. Fröhlich, and C. Jacobi (2007), Planetary waves in coupling the lower and upper atmosphere, *J. Atmos. Sol. Terr. Phys.*, *69*, 2083–2101, doi:10.1016/j.jastp.2007.05.014.

Remsberg, E., G. Lingenfelser, V. L. Harvey, W. Grose, J. Russell, M. Mlynczak, L. Gordley, and B. T. Marshall (2003), On the verification of the quality of SABER temperature, geopotential height, and wind fields by comparison with Met Office assimilated analyses, *J. Geophys. Res.*, *108*(D20), 4628, doi:10.1029/2003JD003720.

Riggin, D. M., D. C. Fritts, T. Tsuda, T. Nakamura, and R. A. Vincent (1997), Radar observations of a 3-day Kelvin wave in the equatorial mesosphere, *J. Geophys. Res.*, *102*, 26,141–26,158, doi:10.1029/96JD04011.

Salby, M. L., and R. R. Garcia (1987), Transient response to localized episodic heating in the tropics. Part I: Excitation and short-time near-field behavior, *J. Atmos. Sci.*, *44*, 458–498, doi:10.1175/1520-0469(1987)044<0458:TRTLEH>2.0.CO;2.

Salby, M. L., D. L. Hartmann, P. L. Bailey, and J. C. Gille (1984), Evidence for equatorial Kelvin modes in Nimbus-7 LIMS, *J. Atmos. Sci.*, *41*, 220–235, doi:10.1175/1520-0469(1984)041<0220:EFEKMI>2.0.CO;2.

Skinner, W. R., et al. (2003), Operational performance of the TIMED Doppler Interferometer (TIDI), *Proc. SPIE Int. Soc. Opt. Eng.*, *5157*, 47–57, doi:10.1117/12.503727.

Sridharan, S., S. Gurubaran, and R. Rajaram (2002), Radar observations of the 3.5-day ultra-fast Kelvin wave in the low-latitude mesopause region, *J. Atmos. Sol. Terr. Phys.*, *64*, 1241–1250, doi:10.1016/S1364-6826(02)00072-X.

Swinbank, R., and D. A. Ortland (2003), Compilation of wind data for the Upper Atmosphere Research Satellite (UARS) Reference Atmosphere Project, *J. Geophys. Res.*, *108*(D19), 4615, doi:10.1029/2002JD003135.

Takahashi, H., C. M. Wrasse, D. Pancheva, M. A. Abdu, I. S. Batista, L. M. Lima, P. P. Batista, B. R. Clemesha, and K. Shiokawa (2006), Signatures of 3–6 day planetary waves in the equatorial mesosphere and ionosphere, *Ann. Geophys.*, *24*, 3343–3350, doi:10.5194/angeo-24-3343-2006.

Takahashi, H., et al. (2007), Signatures of ultra fast Kelvin waves in the equatorial middle atmosphere and ionosphere, *Geophys. Res. Lett.*, *34*, L11108, doi:10.1029/2007GL029612.

Teitelbaum, H., and F. Vial (1991), On tidal variability induced by nonlinear interaction with planetary waves, *J. Geophys. Res.*, *96*, 14,169–14,178, doi:10.1029/91JA01019.

Vincent, R. (1993), Long-period motions in the equatorial mesosphere, *J. Atmos. Terr. Phys.*, *55*(7), 1067–1080, doi:10.1016/0021-9169(93)90098-J.

Wallace, J. M., and V. E. Kousky (1968), Observational evidence of Kelvin waves in the tropical stratosphere, *J. Atmos. Sci.*, *25*, 900–907, doi:10.1175/1520-0469(1968)025<0900:OEOKWI>2.0.CO;2.

Wu, D. L., P. B. Hays, and W. R. Skinner (1995), A least squares method for spectral analysis of space-time series, *J. Atmos. Sci.*, *52*, 3501–3511, doi:10.1175/1520-0469(1995)052<3501:ALSMFS>2.0.CO;2.

Wu, Q., T. L. Killeen, D. A. Ortland, S. C. Solomon, R. D. Gablehouse, R. M. Johnson, W. R. Skinner, R. J. Niciejewski, and S. J. Franke (2006), TIMED Doppler interferometer (TIDI) observations of migrating diurnal and semidiurnal tides, *J. Atmos. Sol. Terr. Phys.*, *68*, 408–417, doi:10.1016/j.jastp.2005.02.031.

Wu, Q., et al. (2008), Global distribution and interannual variations of mesospheric and lower thermospheric neutral wind diurnal tide: 1. Migrating tide, *J. Geophys. Res.*, *113*, A05308, doi:10.1029/2007JA012542.

Wu, Q., S. C. Solomon, Y.-H. Kuo, T. L. Killeen, and J. Xu (2009), Spectral analysis of ionospheric electron density and mesospheric neutral wind diurnal nonmigrating tides observed by COSMIC and TIMED satellites, *Geophys. Res. Lett.*, *36*, L14102, doi:10.1029/2009GL038933.

Yoshida, S., T. Tsuda, A. Shimizu, and T. Nakamura (1999), Seasonal variations of 3.03.8-day ultra-fast Kelvin waves observed with a meteor wind radar and radiosonde in Indonesia, *Earth Planets Space*, *51*, 675–684.

Younger, P. T., and N. J. Mitchell (2006), Waves with period near 3 days in the equatorial mesosphere and lower thermosphere over Ascension Island, *J. Atmos. Sol. Terr. Phys.*, *68*, 369–378, doi:10.1016/j.jastp.2005.05.008.

Zhang, X., J. M. Forbes, M. E. Hagan, J. M. Russell, S. E. Palo, C. J. Mertens, and M. G. Mlynczak (2006), Monthly tidal temperatures 20–120 km from TIMED/SABER, *J. Geophys. Res.*, *111*, A10S08, doi:10.1029/2005JA011504.

Zhou, Q. H., M. P. Sulzer, and C. A. Tepley (1997a), An analysis of tidal and planetary waves in the neutral winds and temperature observed at low-latitude formula E region heights, *J. Geophys. Res.*, *102*, 11,491–11,506, doi:10.1029/97JA00440.

Zhou, Q. H., M. P. Sulzer, C. A. Tepley, C. G. Fesen, R. G. Roble, and M. C. Kelley (1997b), Neutral winds and temperature in the tropical mesosphere and lower thermosphere during January 1993: Observation and comparison with TIME-GCM results, *J. Geophys. Res.*, *102*, 11,507–11,520, doi:10.1029/97JA00439.